Tubular-Shaped Stoichiometric Chrysotile Nanocrystals

Giuseppe Falini,[a] Elisabetta Foresti,[a] Massimo Gazzano,[b] Alessandro F. Gualtieri,[c] Matteo Leoni,[d] Isidoro G. Lesci,[a] and Norberto Roveri*[a, b]

Abstract: Stoichiometric chrysotile tubular nanocrystals have been synthesized as possible starting materials for applications toward nanotechnology, and as a standard reference sample for the investigation of the molecular interactions between chrysotile, the most utilized asbestos, and biological systems. Chrysotile nanocrystals have been synthesized under controlled hydrothermal conditions, and have been characterized by chemical, morphological, structural, spectroscopic and microcalorimetric analyses. They show a constant "cylinder-in-cylinder" morphology constituted by two or three concentric subunits. Each single nanocrystal has a tubular shape of about 49 ± 1 nm in outer maximum diameter, and a hollow core of about 7 ± 1 nm. Structural investigation carried out on an X-ray powder pattern allowed to improve the structural model proposed for chrysotile mineral samples. Synthetic chrysotile crystallizes in the monoclinic *Cc* space group with $a = 0.5340(1)$ nm, $b = 0.9241(1)$ nm, and $c = 1.4689(2)$ nm, $\beta = 93.66(3)°$.

Keywords: chrysotile · health hazard · nanotubes · reference compound · X-ray diffraction

Introduction

Asbestos fiber properties, such as heat resistance, noncombustibility, unusual tensile strength and resistance to selective chemical attack, are important for the wide use of mineral chrysotile in a variety of industrial applications.[1] Chrysotile, which accounts for approximately 95% of manufactured asbestos,[2,3] occurs as a natural fiber that can be woven, moulded, and added to other inorganic and polymeric compounds to form superior and advanced materials with an enhanced value.[4] The silicate mineral chrysotile is also a naturally occurring, nano-sized, tube-shaped material which may represent an alternative to carbon nanotubes for certain applications, such as the manufacture of nanowires.[5,6] The mineral chrysotile nanotubes differ from carbon nanotubes in some important physical parameters, that is, they are nonconducting, they have lower mechanical strength, their length can reach a millimeter range, and they are always uncapped.[7,8]

Health hazards associated with asbestos are well documented in the medical and general health literature, and its deleterious environmental effects are now well-known.[9] Pleural thickening and calcification, pulmonary fibrosis, lung cancer, and pleural mesothelioma are the main health issues associated with asbestos exposure. These pathologies cannot be ascribed exclusively to asbestos fibrous form, and its length to diameter ratio is greater than three.[10] In fact, the chemical, structural, and physico-chemical properties of chrysotile fibers are of major significance in their interactions with biological systems.[11]

Mineral chrysotile, $Mg_3Si_2O_5(OH)_4$ is composed of sheets of Si-centred tetrahedra in a pseudohexagonal network joined to sheets of octahedral magnesium hydroxide (Figure 1). The structure of chrysotile fibrils is composed of layers curved concentrically or spirally, usually around the *x* axis (clinochrysotile and orthochrysotile), and seldom around the *y* axis (parachrysotile), into a tubular structure (rolls) of about 22–27 nm in diameter.[12] The rolls possess hollow cores with a diameter of about 5–8 nm, because the layers cannot energetically withstand too tight a curvature.[13] The earlier X-ray diffraction studies on chrysotile showed a remarkable distortion (curvature) of the unit cell with respect to the conventional crystal structures, so that a

[a] Dr. G. Falini, Prof. E. Foresti, Dr. I. G. Lesci, Prof. N. Roveri
Dipartimento di Chimica "G. Ciamician"
Alma Mater Studiorum University of Bologna
via Selmi2, 40126, Bologna (Italy)
Fax: (+39) 051-209-9456
E-mail: norberto.roveri@unibo.it

[b] Dr. M. Gazzano, Prof. N. Roveri
ISOF-CNR, via Selmi 2
40126 Bologna (Italy)

[c] Prof. A. F. Gualtieri
Dipartimento di Scienze della Terra
Università di Modena e Reggio Emilia
41100 Modena (Italy)

[d] Dr. M. Leoni
Dipartimento di Ingegneria dei Materiali e
Tecnologie industriali, Università di Trento
38050 Mesiano Trento (Italy)

 DOI: 10.1002/chem.200305685

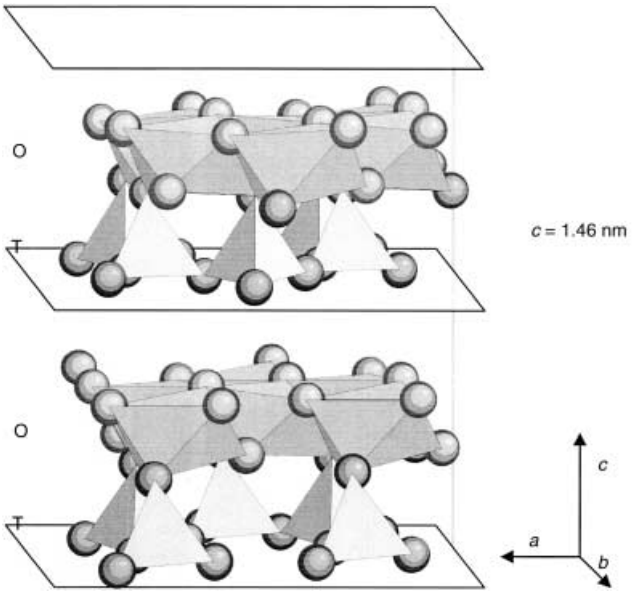

Figure 1. A perspective view of the OT layers in the chrysotile structure. Magnesium environment is represented by octahedra, silicon environment by tetrahedra. The length of the *c* axis is reported.

new theory specially formulated for cylindrical lattices had to be developed.[14–16] The existence of regular cylindrical (or helical) and spiral lattices with a triclinic (anorthic), monoclinic (clinochrysotile[17]), and orthorhombic (clinochrysotile[18] or parachrysotile) symmetry was recognized.

Natural chrysotile fibers may contain different proportions of chrysotile polytypes (*ortho-para*-clino-chrysotile), and mineral samples usually show the intimate intergrowth of the chrysotile polymorphs lizardite and antigorite.[19] Chrysotile fibers are contaminated with other minerals, and trace metals are particularly abundant. In fact, they generally develop as a result of defects in the mineral structure and are subject to many isomorphic substitutions, therefore most fibers contain impurities.[20] These heterogeneities could probably be correlated to the different chrysotile crystal morphologies observed; these include hollow cylinders, nonhollowed cylinder, tube-in-tube fibers, conically wrapped fibers, cone-in-cone-shaped concentric structures, spiral, and multispiral structures.[21]

In natural chrysotile fibers, the tubular crystals have an outer diameter, which ranges from 10 to 50 nm, and an inner diameter between 1 and 10 nm. Its high degree of heterogeneity strongly affects the biological–mineral system interaction; this has been widely investigated in order to individuate the causes of health hazards associated with asbestos.[22,23] For these reasons, the availability of synthetic chrysotile nanotubes with stoichiometric composition, and constant morphology and structure is crucial. Chrysotile nanotubes may be used both as a standard reference sample to investigate the chrysotile features responsible for developing pathologies, and their properties for potential applications in nanotechnology.

Syntheses of chrysotile have been recorded as early as the 1920's and 1930's. Chrysotile has been synthesized by different hydrothermal reactions in the $MgO–SiO_2$ system.[24] The formation of fluorhydroxylchrysotile $Mg_6Si_4O_{10}F_x(OH)_{8-x}$ has been investigated by Ushio and Saito.[25] Olivine was completely serpentinized in the presence of NaOH[26], and transformed firstly into antigorite, which recrystallizes as chrysotile on further reaction in the presence of NaOH, but forms lizardite in the presence of water.[27] Chrysotile microcrystals have been synthesized from olivine and water over a range of different temperature, pressure and time, and [24] various Mg–Ni chrysotile samples have been synthesized by hydrothermal reactions.[28] Chrysotile was obtained by transformation of synthetic diopside $CaMg(Si_2O_6)$.[29] A number of hydrothermal investigations have been made on various assemblages of minerals which make up the serpentine multisystem. These studies are not oriented towards chrysotile syntheses, but rather to the investigation of the reactions, which involve mineral transformations in an attempt to establish stability ranges.[30–33] In the light of the wide availability of asbestos as a natural raw material, the purpose of synthesis may seem somewhat incongruous.[34] Nevertheless, in this paper we present a new approach to synthesize stoichiometric chrysotile regular tube-shaped nanocrystals as a unique phase under controlled hydrothermal conditions.[35] Chemical analysis: X-ray powder diffraction (XRPD), fourier transform infrared spectroscopy (FTIR) and Raman spectroscopy, and scanning electron microscopy (SEM), transmission electron microscopy (TEM), atomic force microscopy (AFM), and microcalorimetric techniques have been used to characterize the synthetic nanocrystals in order to present them as a possible standard reference sample. Their possible applications range from biology to medicine in order to understand the interactions of nanocrystals with biological systems, and for the preparation of quantum wires in nanotechnology.

Results and Discussion

Synthesis and characterization: Stoichiometric chrysotile nanocrystals have been synthesized as a unique phase by means of hydrothermal reactions under controlled conditions. Silica source MCM41 was used instead of the most diffused silica gels for two main reasons: i) commercial silica gel is commonly associated with considerable amounts of metal oxides, and ii) its constant morphology plays a role on the kinetics of the reaction, which ensures a higher reliability. The use of favorable laboratory synthesized MCM41 satisfies the necessary required purity of the reactants in terms of metal ions. This MCM41 showed a average pore size of 3.9 nm and a specific area surface of 910 m^2g^{-1}. The reaction was carried out by using MCM41 in an aqueous solution of $MgCl_2$ with a Si/Mg molar ratio equal to 0.68. The pH was raised to 13.0 by adding NaOH solution, and a hydrothermal treatment at 82 atm for 24 h was then performed. The stoichiometric Si/Mg molar ratio of 0.66 induces the formation of brucite as a second phase, while a Si/Mg molar ratio higher than 0.68 leads to the formation of other silicate compounds such as talc. The optimum value to synthesize chrysotile single phase is pH 13.0; higher values favor the contemporary formation of brucite, while lower values reduce

the chrysotile crystallinity. Reaction times lower than 24 h do not allow chrysotile to reach a high degree of crystallinity. The powder X-ray diffraction pattern of the synthesized chrysotile displays the characteristic reflections of high crystalline chrysotile as a unique crystalline phase (Figure 2a).

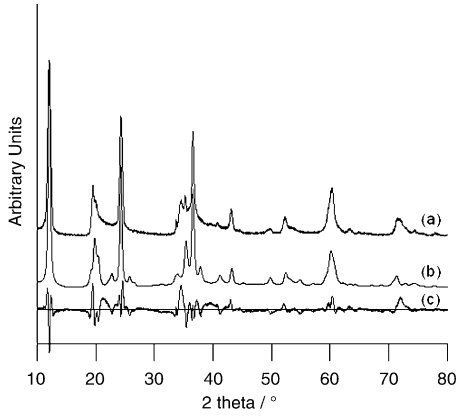

Figure 2. a) Experimental, b) calculated XRPD patterns of the chrysotile nanocrystals, and c) comparison between the observed and the calculated powder patterns.

The TGA and DTA curves of synthetic chrysotile fibers are reported in Figure 3. An endothermic area at 650 °C corresponding to the dehydroxylation of the chrysotile crystals and the sharp exothermic peak at 810 °C indicates the crystallization of the remaining amorphous anhydrous materials (the so-called *meta*-chrysotile $Mg_3Si_2O_7$) into forsterite (Mg_2SiO_4)[36] are observed. The lack of additional peaks, observed in the mineral chrysotile fibers thermal analyses, together with the sharpness of the transformation to forsterite and silica gives evidence for the homogeneity and purity of synthetic chrysotile crystals.

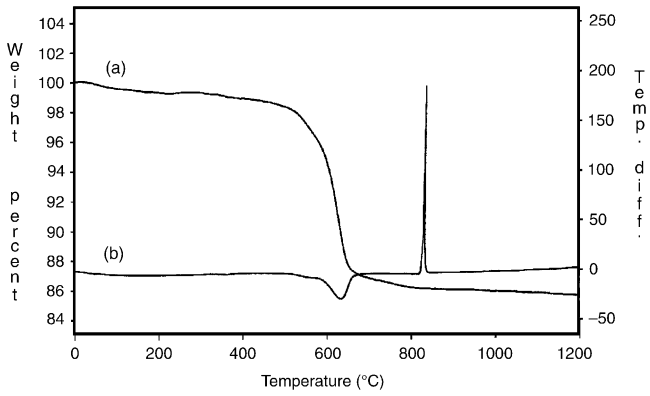

Figure 3. a) TGA and b) DTA scans of synthetic chrysotile fibers.

The synthetic chrysotile main-band frequencies from the FTIR and Raman spectra are reported in Table 1. They agree with literature data,[37,38] and confirm the high purity of the chrysotile, and the absence of other phases. The ICP analysis gives a Si/Mg molar ratio equal to 0.66, as expected for stoichiometric chrysotile. The presence of foreign metals is relegated to very low amounts.

Crystal structure: The peak positions of the observed pattern match those reported on the ICDD file no. 43–662, and unambiguously indicate that the synthetic nanofibres are composed of pure clinochrysotile. Unfortunately, it is known that the space group *C*2/*c* reported on the ICDD file is incorrect.[39] This problem, combined with the observation that the relative intensities were fairly different from those reported in the file, prompted an accurate search for a better space group, a new indexing of the observed pattern, and the structure determination with the Rietveld method. The runs for the unit-cell determination in TREOR[40] clearly indicate a monoclinic setting very similar to the one reported on the ICDD file no. 43–662. A first selection based on systematic absences and peak positions indicated the following possible space groups: *Cc*, *Ca*, *C*2/*c*, which considers a *c* axis of about 1.46 nm and $P2_1$, $P2_1m^{-1}$, and *Cm* considers a *c* axis of about 0.73 nm. The LeBail fits carried out by using the selected space groups clearly indicate three best choices: *Cc*, *C*2/*c*, and $P2_1$. Among these, only *Cc* is consistent with an OT (O = octahedral and T = tetrahedral) layer structure (1:1 tetrahedral and octahedral layer unit; Figure 1). In fact, in the *C*2/*c* space group, whatever the choice of origin may be, one of the layers is invariably doubled in the cell, which generates a TOT or a OTO unit. In the space group $P2_1$, whatever the choice of the origin may be, the symmetry invariably causes an inversion of the polarity of the tetrahedra in the T layer.

The coordinates of an ideal trioctahedral OT unit in the unit cell with $c = 1.46$ nm, space group *Cc*, were used as an input for a Rietveld structure refinement in GSAS.[41] The final agreement factors are $R_p = 23.4\,\%$; $R_{wp} = 26.0\,\%$; $\chi^2 = 5.6$. The refined unit cell parameters are $a = 0.5340(1)$ nm, $b = 0.9241(1)$ nm, $c = 1.4689(2)$ nm, and $\beta = 93.66(3)°$. Figure 2a and b report the observed and calculated powder pattern up to 80° of 2θ. The refined atomic parameters are re-

Table 1. Assignment of the chrysotile FTIR and Raman bands.

FTIR [cm^{-1}]	Assignment	Raman [cm^{-1}]	Assignment
3692	MgOH stretch	3694	external MgOH stretch
3645 (shoulder)	MgOH stretch	3643	internal MgOH stretch
3410 (broad)	H_2O stretch	1102	antisymm. Si–O–Si stretch
1640 (broad)	H_2O bend	690	symm. translation mode Si–O
1082	Si–O–Si stretch	463	
1015	Si–O–Mg stretch	344	Mg–OH symm.translation mode
958	Si–O stretch	231	Mg–O symm. mode
604	Mg–OH libration	431	
435	Si–O–Mg bend	388	Mg–O antisymmetric mode
		315	
		198	

ported in Table 2. The different curve in Figure 2c shows a good degree of agreement between the calculated and the experimental patterns, although the Rietveld algorithm is not specifically designed to take into account curved cylindrical stacking. In any case the model obtained by GSAS program is the preffered choice, because even when a specifically modified version of DIFFaX was used[42] (a suite especially developed to study planar faults in crystals) it was not possible to obtain significantly better results.[43] The structure has been refined by means of GSAS anisotropic broadening parameter along the *b* axis by using the stacking fault model and the following values for the anisotropic Lorentian coefficients: $Lx = 21(1)$ and $stec = 76(1)$.

Table 2. Atomic coordinates for $Mg_3Si_2O_5(OH)_4$ nanocrystals.

Atom type	*x*/a	*y*/b	*z*/c	Occupancy	$U_{iso}[Å^2]$
Mg	0.8852(6)	0.1980(4)	0.2303(4)	1.00	0.007(6)
Mg	0.3747(7)	0.3771(7)	0.2327(5)	1.00	0.007(6)
Mg	0.8818(8)	0.5235(7)	0.2204(7)	1.00	0.007(6)
Si	0.0257(5)	0.3641(8)	0.0410(5)	1.00	0.018(8)
Si	0.5208(5)	0.5335(9)	0.0400(2)	1.00	0.018(8)
O	0.0726(8)	0.1978(5)	0.0000(4)	1.00	0.013(9)
O	0.2387(9)	0.4750(9)	0.0023(3)	1.00	0.013(9)
O	0.7395(9)	0.4214(7)	0.0063(7)	1.00	0.013(9)
O	0.0438(8)	0.3596(7)	0.1560(9)	1.00	0.013(9)
O	0.532(1)	0.537(1)	0.155(1)	1.00	0.013(9)
O(OH)	0.7299(9)	0.363(2)	0.2878(6)	1.00	0.013(9)
O(OH)	0.2395(7)	0.197(1)	0.2791(9)	1.00	0.013(9)
O(OH)	0.5334(8)	0.2053(9)	0.1807(8)	1.00	0.013(9)
O(OH)	0.2025(9)	0.5416(9)	0.296(1)	1.00	0.013(9)

The structural result is very useful because a) it proves that the refined pattern belongs to a pure chrysotile sample; b) it improves the model used for the quantitative phase analysis with the Rietveld method proposed by Gualtieri and Artioli who refined a natural impure standard sample, and[44] c) it fills the void opened in the literature, since Wiks demonstrated the inconsistency of chrysotile space group.[39]

Morphology: The optical microscopy images of synthesized stoichiometric chrysotile show a bundle morphology very close to that of natural chrysotile fibers. SEM images (Figure 4a and b) reveal how the long bundles are constituted of finely matted fibres of a small size (about a few microns long). TEM analysis was carried out on synthetic chrysotile fibers only disaggregated by sonication, without any additional treatment; this reveals the tubular chrysotile single nanocrystals, which aggregate to form microfibers structures (Figure 4c). The single nanocrystals, which have a cylindrical shape with a length of the order of some microns, show a transparency in the central area that run longitudinally along the crystal (Figure 4d). This finding indicates that the crystal core is void or contains low-electron dense material, such as an amorphous phase. The hollow tubular morphology of a chrysotile single crystal is clearly shown in Figure 5(top), in which three tubular subunits are concentrically arranged in a telescopic form. "Cylinder-in-cylinder" morphology is the unique shape observed and the number of concentric tubes is two or three. TEM images indicate that the electron density of crystal walls is nearly uniform and almost continuous along the cylinder axis, while the crystal core has a lower electron density, which suggests the absence of material or the presence of an amorphous phase. A value of about 7 ± 1 nm for the central hole diameter has been determined. A graphical representation of the "cylinder in cylinder" morphology is shown in Figure 5(bottom).

AFM image of the tubular chrysotile nanocrystals is reported in Figure 6a. The mean outer diameter of the tubular chrysotile crystals has been valuated by using the height profile from the AFM image analysis, as shown in Figure 6b. The measured average values are 21 ± 1 nm, 35 ± 1 nm, and 49 ± 1 nm for concentrically arranged tubes, one, two, and three, respectively. These values have been confirmed by measuring the nanocrystals in the TEM images.

The average value of the tube wall thickness is about 7 nm; this was determined by measurements of the nano-

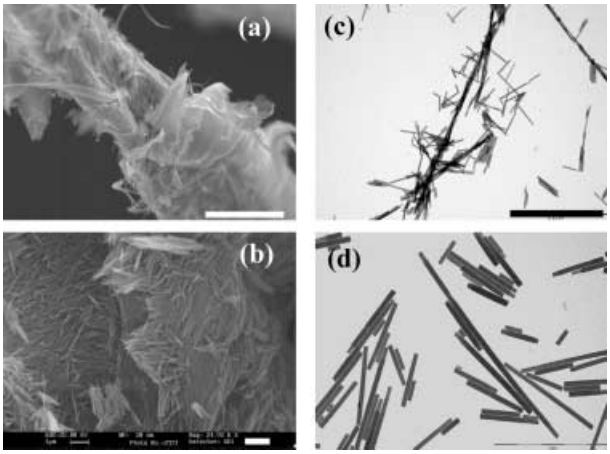

Figure 4. Synthetic chrysotile nanocrystals. a) SEM images: scale bar = 10 μm, b) scale bar = 1 μm, and c) TEM images: scale bar = 2 μm, d) scale bar = 500 nm.

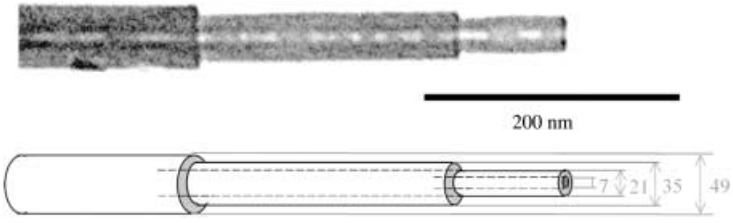

Figure 5. Top: TEM image of a single tubular chrysotile nanocrystal and bottom: graphical representation of the crystal with dimensioning (nm).

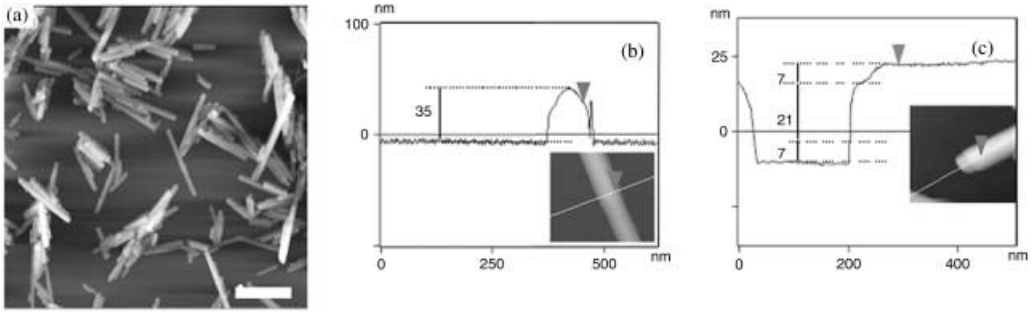

Figure 6. a) AFM image of synthetic chrysotile nanocrystals; scale bar = 500 nm. Height profiles of a nanocrystal constituted by two tubes concentrically arranged: b) perpendicular to the crystal axis and c) along crystal axis, respectively.

crystals in the TEM images and of the AFM height profile, as reported in Figure 6c. The wall thickness of 7 nm of each tube is constant, independent from the fact that the nanocrystal is constituted by one, two, or three concentric tubes. The wall thickness value suggests the presence of about ten OT layers concentrically arranged in every cylindrical unit, in agreement with the layer thickness of 0.73 nm observed in electron diffractions patterns and micrographs by Yada.[12] The value obtained by the crystal structure analysis corresponds to half of the *c* parameter of the unit cell.[15]

Conclusion

Chrysotile nanocrystals have been synthesized under controlled hydrothermal conditions by reacting MCM41 mesoporous silica with $MgCl_2$ in alkaline solution. The synthetic crystals display the characteristic X-ray diffraction pattern of chrysotile as a unique crystalline phase. Stoichiometry has been determined by ICP analysis. The high purity of the synthesized sample was confirmed by microcalorimetric and spectroscopic analysis: DTA and TGA curves, and FTIR and Raman spectra do not show any of the additional peaks/bands usually assigned to impurities associated with mineral chrysotile. The X-ray powder diffraction analysis allowed us to improve the structural model proposed earlier for a mineral sample.[45] The search for the best space group indicates a *Cc* space group with $c = 1.469$ nm, which corresponds to an OT layer thickness of 0.734 nm.

TEM and AFM observations revealed that single nanocrystals have a constant hollow cylindrical morphology. Each nanocrystal is constituted of up to three concentrically arranged tubes and shows an inner channel of about 7 nm in diameter. The tube wall is always formed by about ten concentric octahedra–tetrahedra layers, and it is about 7 nm thick. The nanocrystals tend to aggregate forming fibers. A model based on a "cylinder in cylinder" structural motive has been proposed to explain the different diameter of the nanotubes.

The absence of any poisoning with foreign ions, especially those considered being responsible for asbestos toxicity, suggests that synthetic chrysotile nanocrystals can be used as a possible standard reference sample to investigate chemicophysical properties and interactions with biological systems of mineral chrysotile. Relating the availability of stoichiometric chrysotile nanocrystals with constant morphology and structure allows us to consider the nanotubes as possible starting materials to prepare either quantum wires with optical-electron properties or fibrous materials for innovative applications.

Experimental Section

Materials: All chemicals used were reagent grade. Mesoporous silica MCM41 was prepared by using a sol–gel process according to the method reported by Kresge et al.[45] Tetraethyl orthosilicate (TEOS) was hydrolyzed at an ambient temperature in an aqueous acidic solution by using CTAB as a template. The product was filtrated and washed with water, dried at room temperature, and calcined at 600 °C for 5 h.

Chrysotile synthesis: The synthetic procedure is a modification of the method reported by Noll et al.[24] The hydrothermal synthesis was carried out in a Parr 4564 reactor equipped with a vessel (160 cm^3). For the preparation of nanochrysotile crystals, a gel mixture of MCM41 and $MgCl_2$ in aqueous solution with a Si/Mg molar ratio in the range of 0.6–0.7 was prepared. Its pH was raised to a range of 12–13 by adding aqueous NaOH solution. The final volume was 70 cm^3, and the final concentrations were 10 mM $MgCl_2$ and 0.4 M NaOH. The hydrothermal treatment was carried out at a temperature of 300 °C on the saturated vapor pressure curve (82 atm) with a run duration ranging from 8 h to 3 days. The precipitate removed from the solution was repeatedly washed with deionised water and dried for 3 h at 150 °C.

Inductively coupled plasma atomic emission spectrometry (ICP-AES) analysis: The determination of the elements in the chrysotile crystalline samples was carried out by using ICP-AES Varian Liberty Model 200 instrument. The samples solutions were prepared inside hermetically sealed Teflon holders following two steps: a) HF (1 mL of 48 % wt) and HNO_3 (5 mL 48 % wt) were added to the sample (40 mg) and processed into the mineralizer for 30 min applying 250 Watts (Milestone, model MLS 1200), and b) in order to obtain the formation of the complex with BF_4^-, $Li_2B_4O_7$ (20 mL of 1,8 % wt) was added to preparation a), and processed into the mineralizer for 15 min applying 250 Watts. The sample solutions were then diluted with double distilled water up to 100 mL.

Differential thermal analysis and thermo gravimetrical analysis (DTA-TGA): analysis: DTA-TGA were carried out by using a Polymer Thermal Science STA 1500 instrument. The weight of the samples were in the range of 5–10 mg, and standard pure corundum was used as a reference. Heating was performed in a platinum crucible under a nitrogen flow (20 $cm^3 min^{-1}$) at a rate of 5 °C min^{-1} up to 1200 °C. The heating rate used is in acordance with the reported literature protocol on the DTA-TGA investigation on chrysotile samples[46].

X-ray diffraction analysis: The synthetic chrysotile sample for the X-ray data collection was manually ground in an agate mortar. The powder was mounted on a 1.5 mm thick flat Al holder by using the front loading technique, and the data collection was performed by using a Philips PW 1050/81 powder diffractometer equipped with a secondary graphite monochromator; $Cu_{K\alpha}$ radiation at 40 kV and 40 mA was used. The instru-

ment was configured with a 1° divergence and receiving slits (0.2 mm), respectively.

The presence of impurities was checked and excluded by a preliminary qualitative analysis of the X-ray powder pattern. Phase identification was possible by using the ICDD-PDF-2 database.[47] Cell determination was performed by using the TREOR90 program.[40] The indexing procedure and determination of the space group was possible by means of Chekcell V.4[48] and the LeBail fit procedures in GSAS.[41]

The data set was refined with the Rietveld method by using GSAS. The refinement was carried out according to the following features: a) the background was successfully fitted with a Chebyshev function with nine coefficients; b) the peak profiles were modelled by using a pseudo-Voigt function with one Gaussian and one Lorenzian component with an anisotropic broadening axis (along the *b* axis) by means of the stacking fault model described in GSAS; c) the lattice constants, the phase fractions, and the coefficients corresponding to the sample displacement and asymmetry were also refined. The cut-off value for the calculation of the peak profiles in all refinements was 0.05%, and d) the atomic coordinates and the atomic displacement parameters U_{iso} were also independently refined. Soft constraints with a final weight of 100 were imposed for the Si–O and Mg–O distances, and an overall isotropic atomic displacement parameter was refined for each atomic species. A refinement of the fiber texture was accomplished by using the spherical harmonics correction implemented in GSAS which significantly improved the fit of the profile ($R_p = 18.0\%$, $R_w = 23.3\%$, $\chi^2 = 4.7$). The final texture index by means of a 6th order harmonics correction was 2.725 with the following individual orientation distribution coefficients: (20–2) = 0.074(9), (200) = –0.503(8), (202) = 0.885(7), (40–4) = 2.292(7), (40–2) = –0.493(8), (400) = 0.547(9), (60–2) = 0.427(8), (600) = 1.310(7), (602) = –0.944(8), (604) = –2.29(1), (606) = 0.343(8). Further details of the crystal structure investigation may be obtained from the Fachinformationzentrum Karlsruhe, 76344 Eggestein-Leopoldshafen, Germany (fax +49 7247–808–666; e-mail: crysdata@fiz-karlsruhe.de) on quoting the depository number CSD-413633.

FTIR spectroscopy: The infrared spectra were registered from 4000 to 400 cm^{-1} at 2 cm^{-1} resolution by using a Bruker IFS 66v/S spectrometer. The sample environment atmosphere had a total pressure of 2 mbar of air dried to an atmospheric dew point of −40 °C ($p_{H2O} \approx 13$ Pa) by means of a Balston 76-01 Membrane Air Dryer. Aperture 8 mm, 16 scans, velocity 10 kHz, detector DLATGS, apodization function 3-term Blackman-Harris. Pellets (KBr) were obtained under vacuum by using powdered samples (3 mg) carefully mixed with infrared grade KBr (300 mg).

FT-Raman spectroscopy: The FT-Raman spectroscopic analyses were performed by using a Perkin–Elmer System 2000 FT spectrometer equipped with a Raman accessory, which composed of a Spectron Laser System SL 301 Nd:YAG laser operating a wavelength of 1064 nm. The spectrum of each sample was recorded in triplicate by accumulating 300 scans at 4 cm^{-1} resolution between 400 and 4000 cm^{-1}.

Microscopic investigations: SEM observations were carried out by using a Philips XL-20 scanning electron microscope. The dried chrysotile samples were glued by carbon tape on an aluminum stub and were gold coated.

TEM observations were carried out on samples sonicated for short time in order to slip the aggregates without any additional treatment. A water drop of the chrysotile suspension was transferred onto holey carbon foils supported on conventional copper microgrids. A Philips CM 100 transmission electron microscope operating at 80 kV was used.

AFM observations were carried out on diluted water suspensions of chrysotile adsorbed on freshly cleaved mica at room temperature for 10 min. The mica surface was then thoroughly rinsed with double distilled water and dried under nitrogen flow. A Nanoscope III Multimode (Digital Instruments, Santa Barbara, CA) was used. The samples were imaged in contact mode by using a J scanner and silicon nitride tips (200 μm long with nominal spring constant 0.06 $N\,m^{-1}$). The images were flattened off line by using the digital instrument software program in order to highlight specific features.

Acknowledgment

This work was supported by MIUR (Cofin 2000), CNR and University of Bologna (Funds for Selected Research Topics).

[1] *Asbestos: Properties, Applications, and Hazards. Vol. 2* (Eds.: S. S. Chissick, R. Derricott), John Wiley and Sons, Chichester, UK, **1983**.
[2] M. Ross, "Amphiboles and Other Hydrous Pyriboles-Mineralogy ": *Rev. Mineral*, **1981**, *9A* p. 279.
[3] H. Schreier, in *Asbestos in the Natural Environment*, Elsevier, New York, **1989**, p. 159.
[4] R. L. Perkins, B. W. Harvey, *Method for the Determination of Asbestos in Bulk Building Materials*, EPA-600/R-93/116, **1993**.
[5] A. L. Ivanovskii, *Russian Chemical Reviews* **2002**, *71*, 175–194.
[6] C. Metraux, B. Groberty, P. J. Ulmer, *Mater. Res.* **2002**, *17*, 1129–1135.
[7] H. M. Yates, W. R. Flavell, M. E. Pemble, N. P. Johnson, S. G. Romanov, C. M. Sotomayor-Torres, *J. Cryst. Growth* **1997**, *170*, 611–615.
[8] P. J. F. Harris, *Carbon Nanotubes and Related Structures, New Materials for the Twenty-first Century*; Cambridge University Press, Cambridge, **1999**.
[9] B. T. Mossman, "Health Effects of Mineral Dust": *Rev. Mineral* **1992**, *Vol. 28*, p. 513.
[10] J. P. Leineweber, Dust chemistry and Physics: Mineral and Vitrous Fibres in *Biological Effects of Mineral Fibres*. (Ed. J. W. Wagner), IARC, Sci. Publ. 30, WHO & INSERM, Lyon, France, **1980**, *2*, pp. 881–900.
[11] B. Fubini, C. Otero Arean, *Chem. Soc. Rev.* **1999**, *28*, 373–381.
[12] K. Yada, *Acta Crystallogr. Sect. A* **1971**, *27*, 659–664.
[13] B. A. Cressey, E. J. W. Whittaker, J. W. Eric, *Mineral. Mag.* **1993**, *57*, 729.
[14] E. J. W. Whittaker, *Acta Crystallogr.* **1955**, *8*, 571–574.
[15] H. Jagodzinski, S. N Bagchi, *Neues Jahrbuch fuer Mineralogie* **1953**, 97–100.
[16] B. Devouard, A. Baronnet, *Eur. J. Mineral.* **1995**, 7, 835–846.
[17] E. J. W. Whittaker, *Acta. Crystallogr.* **1956**, *9*, 855–862.
[18] E. J. W. Whittaker, *Acta. Crystallogr.* **1956**, *9*, 862–864.
[19] D. R. Veblen, P. R. Buseck, *Science* **206**, 1398–1400.
[20] F. J. Wicks, D. S. O'Hanley, *Serpentine Minerals: Structures and Petrology, in Hydrous Phyllosilicates* (Ed.: S. W. Bailey), Reviews in Mineralogy, **1988**, p. 19.
[21] K. Yada, K. Iishi, *Am. Mineral.* **1977**, *62*, 958–965.
[22] F. Pott, *IARC* **1980**, *2*, 261–272.
[23] R. P. Nolan, A. M. Oechesle, G. W. Addison, J. Colflesh, in *Mechanisms in Fibre Carcinogenesis* (Ed.: R. C. Brown), Plenum Press, New York, **1991**, p 231.
[24] W. Noll, H. Kircher, W. Sybertz, *Kolloid-Z.* **1958**, *1*, 157–168.
[25] M. Ushio, H. Saito, *J. Chem. Soc. Jpn.* (Industrial Chemistry Section) **1970**, *73*, 1775–1782.
[26] E. N. Korytkova, T. A. , Makarova, *Doklady Earth Sci. Sect.* **1971**, *196*, 144–145.
[27] J. Moody, *Can. Mineral.* **1976**, *14*, 462–478.
[28] H. Koshimizu, S. Higuchi, R. Otsuka, *Clay Sci.* **1981**, *21*, 130–140.
[29] E. Barrese, E. Belluso, F. Abbona, *Eur. J. Mineral.* **1997**, *9*, 83–87.
[30] J. Chernosky, *Am. Mineral.* **1975**, *60*, 200–208.
[31] J. Hemley, J. K. Montoya, C. L. Chryst, P. B. Hosteler, *Am. J. Sci.* **1977**, *277*, 353–383.
[32] M. A. Dungan, *Am. Mineral.* **1977**, *62*, 1018–1029.
[33] W. K. Oterdoom, *Schweiz. Mineral. Petrogr. Mitt.* **1978**, *58*, 127–138.
[34] A. A. Hodgson, in *Asbestos* (Eds.: L. Michaels, S. S. Chissick), Jonh Wiley & Sons, New York, **1985**, pp. 67–114.
[35] G. Falini, E. Foresti, I. G. Lesci, N. Roveri, *Chem. Commun.* **2002**, 1512–1513.
[36] A. Cattaneo, A. F. Gualtieri, G. Artioli, *Phys. Chem. Miner.* **2003**, *30*, 177–183.
[37] E. Foresti, M. Gazzano, A. F. Gualtieri, I. G. Lesci, B. Lunelli, G. Pecchini, E. Renna N. Roveri, *Anal. Bioanal. Chem.* **2003**, *376*, 653–658.
[38] J. T. Kloprogge, R. L. Frost, L. Rintoul, *Phys. Chem. Chem. Phys.* **1999**, *1*, 2559–2577.

[39] F. J. Wicks, *Powder Diffr.* **2000**, *15*, 42 – 50.
[40] P. E. Werner, L. Eriksson, M. Westdahl, *J. Appl. Crystallogr.* **1985**, *18*, 367 – 381.
[41] A. C. Larson, R. B. Von Dreele, *GSAS Generalized structure analysis system*. Laur 86 – 748. Los Alamos National Laboratory, **1994**, Los Alamos, New Mexico.
[42] M. M. J. Treacy, J. M. Newsam, M. V. Deem, *Proc. R. Soc. London* **1991**, *A433*, 499 – 520.
[43] M. Leoni, A. F. Gualtieri, N. Roveri, *J. Appl. Crystallogr.* **2004**, *37*, 166 – 173.
[44] A. F. Gualtieri, G. Artioli, *Powder Diffr.* **1995**, *10*, 269 – 277.
[45] C. T. Kresge, M. E. Leonowicz, W. J. Roth, J. Vartuli, *Nature* **1992**, *359*, 710 – 712.
[46] D. Choquette, *Evaluation Quantitative de la Composition Mineralogique de L'amiante Chrysotile par Thermogravimetrie*, MSc Thesis, University de Sherbrooke, Sherbrooke, Quebec, **1983**.
[47] Powder Diffraction File 2, International Centre for Diffraction Data, **2002**, Newtown Square, Pennnsylvania (USA).
[48] Program distributed by Laboratoire des Matériaux et du Génie Physique, Unité Mixte de Recherche CNRS, Grenoble, France.

Received: November 4, 2003

Published online: April 28, 2004

